WATER RESOURCES RESEARCH, VOL. 49, 1929–1942, doi:10.1002/wrcr.20171, 2013

A risk-based probabilistic framework to estimate the endpoint of remediation: Concentration rebound by rate-limited mass transfer

F. P. J. de Barros,[1] D. Fernàndez-Garcia,[2] D. Bolster,[2] and X. Sanchez-Vila[2]

Received 10 July 2012; revised 30 November 2012; accepted 26 February 2013; published 22 April 2013.

[1] Aquifer remediation is a challenging problem with environmental, social, and economic implications. As a general rule, pumping proceeds until the concentration of the target substance within the pumped water lies below a prespecified value. In this paper we estimate the a priori potential failure of the endpoint of remediation due to a rebound of concentrations driven by back diffusion. In many cases, it has been observed that once pumping ceases, a rebound in the concentration at the well takes place. For this reason, administrative approaches are rather conservative, and pumping is forced to last much longer than initially expected. While a number of physical and chemical processes might account for the presence of rebounding, we focus here on diffusion from low water mobility into high mobility zones. In this work we look specifically at the concentration rebound when pumping is discontinued while accounting for multiple mass transfer processes occurring at different time scales and parametric uncertainty. We aim to develop a risk-based optimal operation methodology that is capable of estimating the endpoint of remediation based on aquifer parameters characterizing the heterogeneous medium as well as pumping rate and initial size of the polluted area.

Citation: de Barros, F. P. J., D. Fernàndez-Garcia, D. Bolster, and X. Sanchez-Vila (2013), A risk-based probabilistic framework to estimate the endpoint of remediation: Concentration rebound by rate-limited mass transfer, *Water Resour. Res.*, *49*, 1929–1942, doi:10.1002/wrcr.20171.

1. Introduction

[2] Pump-and-treat is a process where contaminated groundwater is extracted from the subsurface by pumping and then in principle treated before it is discharged or reinjected into the aquifer. It is probably one of the most common forms of groundwater remediation at polluted sites [e.g., *Mackay and Cherry*, 1989; *Zhang and Brusseau*, 1999]. Despite its common use, several studies have shown that as currently designed it often fails. For example, the *National Research Council* [1994] studied 77 sites where pump-and-treat was applied and identified that it failed to properly remediate these sites in 69 of those sites. One explanation for the failure is that the pumping process effectively removes contaminants from the most mobile zones in the subsurface, while high levels of contamination can persist in relatively immobile regions [*Soga et al*., 2004].

[3] Concentration signals in the well at early times are associated with preferential flow paths, while concentrations at late times are mostly controlled by the less conductive areas. Thus, while the concentrations of water arriving at the pumping well might decrease below some desired threshold, once pumping stops, an exchange of contaminant between mobile and less mobile zones (e.g., low permeability zones and/or stagnant zones) could take place leading to a rebound in water concentrations [e.g., *Cohen et al*., 1994; *Harvey et al*., 1994; *Luo et al*., 2005, 2006]. This is demonstrated schematically in Figure 1, which shows the effect of pumping on the concentration signal at the well (see *withdrawal stage* and *resting stage*). During the initial stage, the flux-averaged concentration [e.g., *Kreft and Zuber*, 1978; *van Genuchten and Parker*, 1984] at the well decreases with time. This does not imply a reduction of the resident concentration since most of the solute remains in the low mobility regions (denoted *immobile* regions). This mass is transferred to the more permeable zones by diffusion or desorption processes [*Haggerty and Gorelick*, 1995].

[4] The occurrence of rebound concentrations has important implications for the use of pump-and-treat strategies [e.g., *Harvey et al*., 1994]. In order to truly remediate a site, one may have to pump for a significantly longer period when compared to the time estimated assuming all solutes are fully mobile. This means that a particular site could potentially remain contaminated for a longer time than initially expected, resulting in serious economic consequences both in terms of having to run the remediation process for longer times and the fact that the site will remain unavailable for other uses until cleanup is achieved.

[1]Sonny Astani Department of Civil and Environmental Engineering, University of Southern California, Los Angeles, California, USA.
[2]Department of Geotechnical Engineering and Geosciences, Technical University of Catalonia (UPC), Barcelona, Spain.
[3]Civil and Environmental Engineering and Earth Sciences, University of Notre Dame, Indiana, USA.

Corresponding author: F. P. J. de Barros, Sonny Astani Department of Civil and Environmental Engineering, University of Southern California, Kaprielian Hall, Room 224B, 3620 S. Vermont Avenue, Los Angeles, CA 90089-2531, USA. (fbarros@usc.edu)

0043-1397/13/10.1002/wrcr.20171

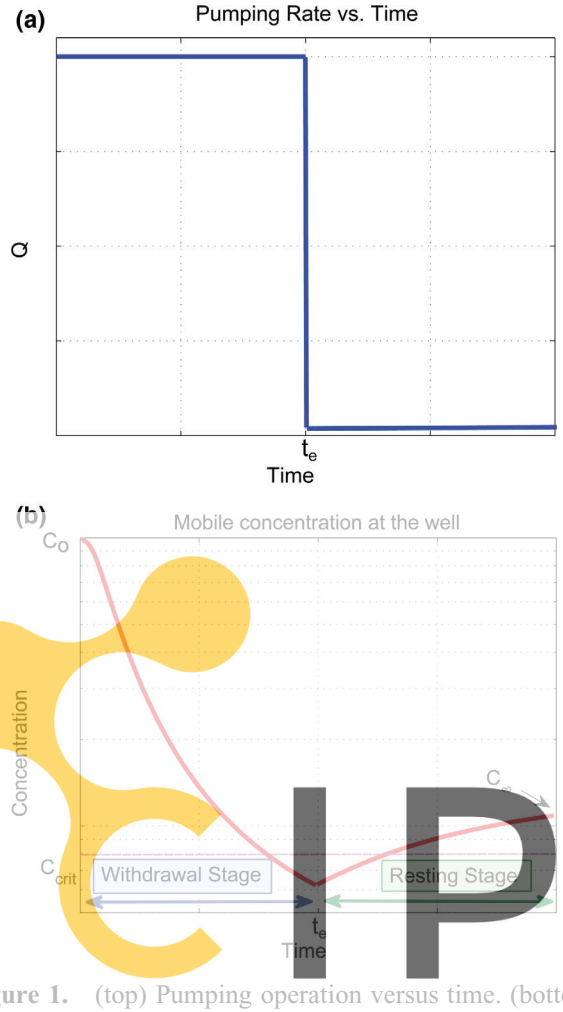

Figure 1. (top) Pumping operation versus time. (bottom) Concentration signal response to pumping operation and mass transfer processes occurring within the domain and the pumping well is activated to remediate the problem (top). Once the concentration level decreases (bottom, withdrawal stage), the pumping well is turned off. A rebound occurs (bottom, resting stage), and the concentration can rise with time toward a value C_∞ which could exceed a given critical concentration C_{crit} (marked by the horizontal dashed line).

[5] In many real systems it can be practically difficult to model in full detail all the complex processes that occur in the subsurface. This is due to lack of characterization data and the natural occurrence of variability. Given these challenges, a variety of effective models that aim to capture the role of heterogeneity have arisen. From all the available models, we choose to work with the multirate mass transfer (MRMT) [e.g., *Haggerty and Gorelick*, 1995; *Carrera et al.*, 1998] as it is developed conceptually and explicitly from the idea that mass is transferred between a mobile zone and a suite of immobile zones. Such models have also been shown to properly incorporate desorption processes [*Lawrence et al.*, 2002] and tested in the field [*Meigs and Beauheim*, 2001; *Haggerty et al.*, 2001; *McKenna et al.*, 2001; *Gouze et al.*, 2008; *Ma et al.*, 2010]. Thus, in our opinion, it provides a framework to model rebound of concentrations driven by back diffusion in pump-and-treat scenarios.

[6] It is important to note that a deterministic estimate of the rebound concentration is typically unfeasible due to lack of subsurface characterization [e.g., *Rubin*, 2003]. Therefore, uncertainty quantification of the rebound concentration is an important component that should be incorporated in a remediation framework.

[7] In this work we develop a risk-based modeling framework, based on the MRMT approach, with the goal of properly studying a pump-and-treat system that is capable of capturing concentration rebound events that have to date lead to failure of remediation efforts. The important contribution of this paper comes from the fact that we present a new risk-based framework capable of estimating the endpoint of pump-and-treat remediation methods and corresponding uncertainty. We provide a flexible framework that could be used to design optimal pumping tasks while accounting for the risk of rebound occurrence. This work is unique in the sense that it unites uncertainty quantification with the use of an upscaled model (MRMT) to estimate the risk of a rebounding event to be above some critical concentration. We highlight the following outcomes of our work:

[8] We derive closed-form expressions to estimate the concentration rebound at the pumping well that account for back diffusion with different memory functions. These expressions allow for a better understanding of the parameters controlling the magnitude of the rebound concentration.

[9] We provide a stochastic evaluation of the rebound concentration conducive to estimating the probability that the rebound concentration will exceed some regulatory critical value.

[10] The probabilistic modeling framework developed in this paper can help address the following challenging questions: How long should we pump in order to minimize the risk of the rebound concentration exceeding a critical concentration value? What is the uncertainty associated with the risk of such an undesired event occurring? How does risk decrease with the intrinsic mass transfer processes taking place within the aquifer?

[11] In section 2, we introduce our conceptual setup and model development. Section 3 provides analytical solutions for the rebound concentration under idealized, but justifiable, approximations. Section 4 explores the model by considering two different but often used memory functions for the MRMT model, namely, the single-rate and power-law distribution of rates. In section 5, we perform a probabilistic analysis by accounting for uncertainty in the MRMT parameters. An analytical derivation of the rebound concentration probability density function (PDF; accounting for parametric uncertainty) is provided. In section 6, we show how to use the stochastic model described with data from a field site. This section will help to illustrate the potential applicability of our model. Finally, we provide a summary in section 7.

2. Problem Formulation

2.1. Definitions

[12] We are interested in better understanding the controlling factors influencing concentration rebounds after

shutting down of a pumping well and the associated risk of concentration being above a regulatory value denoted here as C_{crit}. The ultimate goal is to develop a capacity to provide a priori estimates of pumping time and flow rate that could result in a remediated aquifer given a degree of certainty. The different stages of the problem investigated are outlined in Figure 1.

[13] We start with a large contaminant plume being detected within an aquifer. After detection, a pumping well is installed and the concentration C [ML^{-3}] is monitored at the source zone of contamination. The well is put into operation at a volumetric rate Q [L^3T^{-1}] (withdrawal stage, see Figure 1), and C of the outflow water is recorded as a function of time. After some time of pumping, t_e [T], when the concentration C has dropped to some prespecified value, the pumping well is shut down ($Q = 0$). Mass is mostly lowered in the permeable areas such that when pumping ceases, the system is not equilibrated in terms of concentration. Thus, due to diffusive mass transfer from the immobile zones to the mobile zone, the concentration signal starts increasing (resting stage, see Figure 1) producing a characteristic rebound effect. Note that the withdrawal and resting stages could be repeated in cycles [see *Harvey et al.*, 1994; *MacKay et al.*, 2000].

[14] Our focus is on the concentration evolution in time at the pumping well during the withdrawal and resting stages. As contaminated water is pumped from the aquifer at location $\mathbf{x}_w$ [L], the concentration signal decays with time to a given value that depends on t_e, e.g., $C(\mathbf{x}_w, t_e)$.

[15] When pumping ceases, concentration values rebound, increasing with time until eventually reaching a maximum value C_∞ [ML^{-3}]. This C_∞ value is a function of the natural system, the initial distribution of the concentration, the total mass, and finally, the management operation (through Q and t_e).

[16] Due to the heterogeneity inherent in hydrogeological modeling, decision makers are interested in quantifying the probability that $C_\infty \geq C_{\text{crit}}$. If such an event occurs, then measures need to be taken to continue cleanup at the site. Here C_{crit} corresponds to a threshold concentration based on public health studies and established by a regulatory agency [e.g., *U.S. Environmental Protection Agency*, 2001]. Therefore, risk is defined here as

$$\text{Risk}(\mathbf{x}_w|t_e) = \Pr\left[C_\infty(\mathbf{x}_w|t_e) \geq C_{\text{crit}}\right]. \tag{1}$$

[17] The challenge lies in being able to estimate C_∞ based on t_e, Q, and the properties that define the hydrogeological characteristics of the aquifer. Note that in equation (1), C_∞ is assumed to be time independent. In reality, after the initial rebounding buildup, the concentration signal at the well can decrease with time due to natural attenuation or even shift due to ambient flow. For our work, we assume that the time scale of natural attenuation is very large compared to the time needed for C_∞ to reach a *plateau*. In other words, natural attenuation will be present but acting on a slower time scale. Following a conservative approach within a risk-based framework, we neglect the contribution of natural attenuation in the cleanup process. Under this condition, C_∞ is an asymptotic value and can correspond to a worst-case scenario (aligned with a conservative risk approach). Under this assumption, the rebound concentration, conditional on t_e, can be expressed as

$$C_\infty(\mathbf{x}_w|t_e) = \lim_{t\to\infty} C(\mathbf{x}_w, t), \qquad \forall t \geq t_e. \tag{2}$$

2.2. Conceptual Model

[18] For this work, we want a modeling approach that accounts for transport in heterogeneous media by means of an upscaled equation. We chose to use the MRMT model. The MRMT modeling approach explicitly accounts for the diffusive exchange between mobile and immobile zones that can lead to the concentration rebounds of concern. The use of the MRMT model as a valuable and convenient upscaled transport equation has been shown in many papers [*Haggerty and Gorelick*, 1995; *Willmann et al.*, 2008; *Fernàndez-Garcia et al.*, 2009]. It has been employed to model fate and transport through heterogeneous porous media and is very flexible in capturing complex behaviors [*Chen and Wagenet*, 1995; *Lawrence et al.*, 2002] and interpreting tracer tests in the field [*Meigs and Beauheim*, 2001; *Haggerty et al.*, 2001; *McKenna et al.*, 2001; *Gouze et al.*, 2008; *Ma et al.*, 2010]. It can also address transport of reactive solutes [*Donado et al.*, 2009; *Willmann et al.*, 2010], which could be of potential interest for remediation strategies of complex chemicals, a topic we deem to be beyond the scope of our current study. The general equations of transport for the MRMT can be written as (see works by *Carrera et al.* [1998] and *Haggerty et al.* [2000b] for additional details)

$$\theta_m \frac{\partial C_m}{\partial t} + \int_0^\infty \theta_{\text{im}}(\alpha) \frac{\partial}{\partial t} C_{\text{im}}(\alpha) \mathrm{d}\alpha = -\mathbf{q}\nabla C_m + \nabla \cdot [\mathbf{D}_o \nabla C_m] \tag{3}$$

$$\frac{\partial}{\partial t} C_{\text{im}}(\alpha) = \alpha [C_m - C_{\text{im}}(\alpha)] \tag{4}$$

with C_m [ML^{-3}] representing the concentration in the mobile zone and $C_{\text{im}}(\alpha)$ [ML^{-3}] representing the concentration in the immobile zone, both expressed as mass per unit volume of water (we emphasize here that the term *immobile* is a qualitative term since it can physically represent low mobility zones). The specific discharge vector is given by $\mathbf{q}$ [LT^{-1}], $\mathbf{D}_o$ [L^2T^{-1}] is the local-scale dispersion tensor, and α [T^{-1}] is a mass transfer rate coefficient characterizing the immobile zone, which in the MRMT formulation can take on multiple values. θ_m and $\theta_{\text{im}}(\alpha)$ are the porosities of the mobile and immobile zones, respectively. In the latter, α is also used for the parameterization of $\theta_{\text{im}}(\alpha)$. Solving equation (4), we get

$$C_{\text{im}}(\mathbf{x}, t, \alpha) = \int_0^t \alpha \exp[-\alpha(t-\tau)] C_m(\mathbf{x}, \tau) \mathrm{d}\tau + C^o_{\text{im}}(\mathbf{x}, \alpha) \exp[-\alpha t], \tag{5}$$

where $C^o_{\text{im}}(\mathbf{x}, t, \alpha)$ is the initial concentration for an individual immobile zone. Let ρ_{im} be the contaminant mass in

the immobile zone per total unit volume of aquifer at a given location and time, i.e.,

$$\rho_{\text{im}}(\mathbf{x},t) = \int_0^\infty \theta_{\text{im}}(\alpha) C_{\text{im}}(\mathbf{x},t,\alpha)\mathrm{d}\alpha. \tag{6}$$

[19] Note that $\theta_{\text{im}}(\alpha)$ reflects a distribution, continuous or discrete, of multiple mass exchange rates α, and it is assumed constant in space. Using equation (5), ρ_{im} can be written as

$$\rho_{\text{im}}(\mathbf{x},t) = \int_0^t C_m(\mathbf{x},\tau) g(t-\tau)\mathrm{d}\tau + \int_0^\infty \theta_{\text{im}}(\alpha) C^o_{\text{im}}(\mathbf{x},t,\alpha)\exp[-\alpha t]\mathrm{d}\alpha, \tag{7}$$

where $g(t)$ denotes what is called the memory function, defined as

$$g(t) = \int_0^\infty \alpha\theta_{\text{im}}(\alpha)\exp[-\alpha t]\mathrm{d}\alpha. \tag{8}$$

[20] The memory function is a key component of the MRMT model, and its structure is what ultimately controls the complex concentration dynamics in a given system. A wide variety of memory functions have been proposed reflecting a variety of rate distributions ranging from single first order, multiple discrete first order, Gamma or power-law distributed [e.g., *Haggerty et al.*, 2000b]. One of the interesting features of this model is the rich dynamics that can emerge due to the wide range of memory functions and corresponding behaviors that can be observed. In particular cases, such as the presence of a memory function that depends only on time, the MRMT shares a large number of similarities with the continuous time random walk (CTRW) approach [*Dentz and Berkowitz*, 2003]. Many works have been able to show that the CTRW works effectively in reproducing lab and field data [e.g., *Berkowitz et al.*, 2006].

3. Approximate Solution

3.1. Assumptions and Especial Cases

[21] From a practical perspective it is often necessary to solve the equations presented so far in a seminumerical or fully numerical manner [e.g., *Haggerty et al.*, 2000a]. For the problem at hand we are most interested in predicting C_∞. To develop a fully analytical solution for this problem we invoke some simplifying assumptions, which we summarize below:

[22] *High Péclet*: We assume that the pumping rate from the aquifer Q is sufficiently large that advection is the main transport mechanism in the mobile zone. Based on this we assume (to first order) that it is reasonable to neglect the effect of local-scale dispersion ($\mathbf{D}_o \approx 0$). Therefore we consider only problems where advection dominates the system (in the mobile zone). This is because pumping increases the dominance of advection. The whole aim of pumping is to mobilize water to the well; this suggests that for a well designed system the advection process should indeed dominate during the pumping process. It is important to note that the only relevant mass transfer process in the immobile zone is diffusion.

[23] *Late-time approximation: Haggerty et al.* [2000b] argued that at late times it is reasonable to assume that concentrations do not change significantly over time. This assumption implies that at late times, concentrations are driven by mass exchange (by diffusion) between mobile and immobile zones.

[24] *One-dimensional radial system*: We assume that the pump-and-treat process is placed in the center of the contaminant plume that is sufficiently large and uniform to assume radial symmetry. Although the expressions we develop are for a radial flow configuration, they can also be written for uniform-in-the-mean flow conditions.

[25] Using the first two assumptions we can approximate ρ_{im} with

$$\rho_{\text{im}}(\mathbf{x},t) \approx g(t) m_o + \int_0^\infty \theta_{\text{im}}(\alpha) C^o_{\text{im}}(\mathbf{x},t,\alpha)\exp[-\alpha t]\mathrm{d}\alpha, \tag{9}$$

where m_o is the zeroth moment of the breakthrough curve (see more details in *Haggerty et al.* [2000b]). Invoking the third assumption, the MRMT governing equation (3) for the mobile concentration can be simplified as

$$\frac{\partial C_m}{\partial r} = -\frac{1}{v\theta_m}\frac{\partial \rho_{\text{im}}}{\partial t}, \tag{10}$$

where $v = q/\theta_m$. Since under the late-time assumption ρ_{im} is no longer a function of r, equation (10) can be solved, and the mobile concentration at the well location is

$$C_m(\mathbf{x}_w,t) = -\frac{t_{\text{adv}}}{\theta_m}\frac{\partial \rho_{\text{im}}}{\partial t}, \tag{11}$$

where $t_{\text{adv}} \equiv \int_{r_w}^{R} v^{-1}\mathrm{d}r$ is the advective time over radius R, and r_w denotes the well radius. The parameter R can represent an estimate of the extent of contamination. Taking $v = Q/2\pi r b\theta_m$ and assuming that $R \gg r_w$ we approximate the advection time as

$$t_{\text{adv}} = \frac{\pi R^2 b\theta_m}{Q}, \tag{12}$$

with b [L] denoting the formation's thickness. Differentiating equation (9) and substituting into equation (11), the concentration within the mobile phase can be calculated as

$$C_m(\mathbf{x}_w,t) = -\frac{t_{\text{adv}}}{\theta_m}\left[m_o\frac{\partial g}{\partial t} + \frac{\partial}{\partial t}\int_0^\infty \theta_{\text{im}}(\alpha) C^o_{\text{im}}(\alpha)\exp[-\alpha t]\mathrm{d}\alpha\right]. \tag{13}$$

[26] Equation (13) provides the late-time solution for the withdrawal phase concentration. To obtain an estimate for C_∞, we assume that the system is fully mixed

(concentrations in the mobile and immobile domains at a given point are equal). Thus, by mass balance we obtain

$$C_\infty(\mathbf{x}_w|t_e) = \frac{\theta_m C_m(\mathbf{x}_w, t_e) + \rho_{\text{im}}(\mathbf{x}_w, t_e)}{\theta_{\text{tot}}}, \tag{14}$$

where the total porosity is given by $\theta_{\text{tot}} = \theta_m + \int \theta_{\text{im}}(\alpha)\mathrm{d}\alpha$.

[27] Equation (14) is a conservative estimate that will yield results greater than actual values. From equation (14), it should be clear that initial conditions in the immobile concentration can play an important role in the final result (see equation (9)). Thus, we will consider two end-member cases for initial conditions to test the extremes. These will correspond to *young* and old contaminated sites. By young, we mean that the spill was sufficiently recent such that no concentration has had time to enter the immobile zone. By old, we mean that the spill occurred sufficiently long ago such that the immobile and mobile concentrations are in equilibrium and thus equal. Any other intermediate scenario should lie between these two extremes. Therefore, evaluating the rebound concentration for both setups (young and old) provides end-member cases and thus an upper and lower bound on the cleanup times. This is informative within a risk context since it is inherently difficult to obtain a detailed characterization of the initial and boundary conditions. The assumption of young and old sites can be relaxed in the presence of available computational power to perform simulations along with detailed site information.

3.1.1. Young Contaminated Site

[28] By our definition of a young contaminated site, $C^o_{im} = 0$. Thus, combining equations (9), (13), and (14) results in

$$C_\infty = \frac{1}{\theta_{\text{tot}}}\left(g(t)m_o - t_{\text{adv}}\, m_o \frac{\partial g}{\partial t}\right)\Big|_{t=t_e}, \tag{15}$$

which can readily be evaluated at t_e, the end of pumping time. Recall that m_o is the zeroth-order moment of the breakthrough curve.

3.1.2. Old Contaminated Site

[29] Similarly, by our definition of an old contaminated site, $C^o_{\text{im}} = C^o_m = C_o$. Substituting equations (13) and (9) into equation (14) yields

$$C_\infty = \frac{g(t)m_o}{\theta_{\text{tot}}} + \frac{C_o}{\theta_{\text{tot}}}h(t) - \frac{t_{\text{adv}}\, m_o}{\theta_{\text{tot}}}\frac{\partial g}{\partial t} - \frac{t_{\text{adv}}\, C_o}{\theta_{\text{tot}}}\frac{\partial h}{\partial t}, \tag{16}$$

where

$$h(t) = \int_0^\infty \theta_{im}(\alpha)\exp[-\alpha t]\mathrm{d}\alpha \equiv \int_t^\infty g(\tau)\mathrm{d}\tau. \tag{17}$$

[30] Executing the integrals, this can be simplified and evaluated at time t_e as

$$C_\infty = \frac{1}{\theta_{\text{tot}}}\left[g(t)m_o + C_o h(t) - t_{\text{adv}}\, m_o \frac{\partial g}{\partial t} + t_{\text{adv}}\, C_o g(t)\right]\Big|_{t=t_e}, \tag{18}$$

which is similar to the young site expression in equation (15) with two additional terms reflecting the different initial condition.

3.2. Discussion

[31] Equations (15) and (18) can be used to obtain a preliminary deterministic estimate of the time needed for aquifer remediation. This could be applied to obtain an estimate of the cleanup time used to evaluate the potential cost of the remediation effort for a given Q value (which is a design variable). Thus, a predesign of a remediation system can be performed using the equations for C_∞. For the given approach described in the previous section, the way to proceed involves the evaluation of the following parameters:

[32] *The memory function g(t)*: The memory function can be estimated from either knowledge of the system or more generally, from the interpretation of tracer tests at the site or in a laboratory. A model could also be prespecified and then could be tested for different combinations of parameters.

[33] *The zeroth moment of the breakthrough curve* m_o can be estimated by evaluating the ratio between the initial mass in the system, based on a number of existing measurements or on the information of the total mass spilled, and the pumping rate. For more details, see *Haggerty et al.* [2000b].

[34] *The total porosity* θ_{tot} could be obtained from existing data from outcrops or else by an estimate based on the geology of the site.

The advective time t_{adv}: Its estimation depends on the geometry of the aquifer (with thickness b) and the pumping rate Q (the design variable).

[35] By setting $C_\infty = C_{\text{crit}}$, a curve Q versus t_e could be obtained. Such a curve would allow one to determine an optimal combination (Q, t_e) that minimizes the financial costs involved; this could be achieved by providing an economic model accounting for Q (which can be translated to terms of energy costs) and t_e (duration of the energy costs plus the opportunity costs involved in the fact that the site cannot be used until cleanup is completed). Additional restrictions could be included, such as the need to limit the value of Q so as to reduce drawdown or to increase pump efficiency.

[36] It is important to emphasize that the ideas put forth in this work (as well as the upcoming results) are not limited to the MRMT model. Our choice is to work in a fully analytical framework. However, numerical approaches could be used to relax the assumptions we invoke and to capture more complex heterogeneity patterns [see *Carrera et al.*, 1998; *Silva et al.*, 2009]. Alternative approaches using upscaled models such as the stochastic advection dispersion equation [*Morales-Casique et al.*, 2006], Lagrangian models of anomalous transport [*Cushman and Ginn*, 1993], the CTRW [*Berkowitz et al.*, 2006], and the fractional advection dispersion equations [*Benson et al.*, 2001] could also be used within our framework. For a review and discussion of these approaches and the similarity between all of these models, see *Dentz and Berkowitz* [2003], *Margolin et al.* [2003], and *Neuman and Tartakovsky* [2009]. In addition, a suite of full-blown numerical Monte Carlo simulations could also be applied, say if the setup or boundary conditions do not allow for a closed-form solution

[*Maxwell et al.*, 2008]. Implementing the problem from a numerical perspective would also be a convenient way to take into consideration nonsmooth heterogeneities.

[37] The analysis presented in this work considers the presence of a single pumping well. In practice, multiple wells might be used. The methodology and solution provided will not change if these multiple wells are located far away from one other in such a manner that they do not interfere (or that the interference can be neglected). In the event of interference, our analytical solution could be seen as an upper bound. In any case, for a complete solution with multiple wells, one would have to solve the governing equation numerically and then include the solution in the risk analysis.

[38] In the following sections, we will quantitatively illustrate how the expressions derived in section 3 can be used to (1) better understand the mechanisms controlling the magnitude of C_∞ and (2) estimate the probability of $C_\infty > C_{crit}$ (i.e., risk of remediation failure, see equation (1)).

4. Impact of the Memory Function on the Rebound Concentration

[39] This section will focus on illustrating the influence of the memory function $g(t)$ on C_∞. We will concentrate on two different, but often applied, memory function models, corresponding to a single-rate mass transfer and a power-law distribution of rates. We will explore how their parameters affect C_∞. For illustrative purposes, we will focus on our solution assuming that the contaminated site is young (i.e., equation (15)). The parameter values used in the simulations are listed in Table 1.

4.1. Single-Rate Mass Transfer Model

[40] Let us consider the case of a single-rate mass transfer model, which is typically applied to represent diffusion-controlled mass transfer between mobile and immobile zones. This corresponds to an immobile porosity distribution $\theta_{im}(\alpha) = \theta^0_{im}\delta[\alpha - \alpha_0]$, where θ^o_{im} is the total porosity of the immobile zone and δ is the Dirac δ operator. Using this expression and equation (8), the memory function becomes

$$g(t) = \alpha_o \theta^o_{im} \exp[-\alpha_o t]. \tag{19}$$

[41] Differentiating this expression and substituting into equation (15) yield the following closed-form solution for the rebound concentration

$$C_\infty = \frac{m_o \alpha_o \theta^o_{im}}{\theta_{tot}} (1 + t_{adv}\,\alpha_o)\exp[-\alpha_o t_e], \tag{20}$$

which can now be evaluated for a given setup.

Table 1. Parameter Values Used in the Simulations

Parameter Values	
Zeroth-order moment of the breakthrough curve m_o	1 h kg m^{-3}
Mobile porosity θ_m	0.14
Immobile porosity θ_{im}	0.21
Radius of the contaminated area R	10 m
Pumping rate Q	10 m^3 d^{-1}
Aquifer thickness b	5 m

[42] From equation (20) we note that C_∞ decays exponentially with pumping time. This rate of exponential decay is governed by the rate α_o, i.e., the larger the value of α_o the faster the decrease in C_∞. This reflects that large values of α imply fast exchange between mobile and immobile zones, so that the latter are flushed more quickly. C_∞ is directly proportional to m_o (i.e., zeroth moment of the breakthrough curve) and to $\theta^o_{im}/\theta_{tot}$, the fraction of immobile to total porosity in the system, reflecting what fraction of the mass is available to the immobile zone, eventually causing the rebound. Finally, C_∞ is also proportional to $1 + t_{adv}\,\alpha_o$; large values of t_{adv} reflect either larger plumes or small pumping rates, thus resulting in large times needed to flush the system. Higher values of α_o result in larger rebound concentrations at early times, which results in an interesting competition between the early time constant value and exponential decay, which dominates later times.

[43] Figure 2 (top half) depicts the evolution of C_∞ with t_e for various values of α_o spanning several orders of magnitude. The influence of the individual parameters discussed in the previous paragraph is visible in Figure 2. Parameter values are listed in Table 1 and in the caption of Figure 2.

[44] As one would expect from equation (20), C_∞ values decrease exponentially with an increase of t_e; however, its rate of decrease depends on α_o. After a certain threshold value for t_e, C_∞ decreases with a steep gradient. This is more pronounced for larger α_o. For $\alpha_o = 10^{-3}$d^{-1}, a constant value for C_∞ persists for values of t_e up to 3×10^3 days (approximately 8 years). This implies high costs associated with pumping operations for contaminated sites that have small mass transfer rates between mobile and immobile zones.

[45] The bottom half of Figure 2 is a contour plot of C_∞ for various t_e and α_o. This plot illustrates the nonmonotonic behavior in α_o. The dark black line is an isocontour corresponding to $C_\infty = 0.35$ mg L^{-1}, which was defined as a threshold for risk (i.e., $C_\infty = C_{crit}$). The nonmonotonic behavior in α_o demonstrates how uncertainty in α_o may lead to significant uncertainty in risk assessment.

4.2. Power Law

[46] Next we consider a power-law distribution of α, which might be associated with systems that display strong power-law tailing in breakthrough curves, frequently observed in field and laboratory studies. The power-law model implies [e.g., *Haggerty et al.*, 2000b]

$$\theta_{im}(\alpha) = \mathcal{A}\theta^{tot}_{im}\alpha^{k-3} \qquad \text{with } \mathcal{A} = \frac{k-2}{\alpha^{k-2}_{max} - \alpha^{k-2}_{min}}, k > 0, k \neq 2; \tag{21}$$

k represents the power-law exponent, and α_{min} and α_{max} are the minimum and maximum cutoffs, respectively. The corresponding memory function (equation (8)) is given by

$$\begin{aligned} g(t) &= \mathcal{A}\theta^{tot}_{im}\int_{\alpha_{min}}^{\alpha_{max}} \alpha^{k-2}\exp[-\alpha t]\mathrm{d}\alpha \\ &= \theta^{tot}_{im}\mathcal{A}t^{1-k}\{(\Gamma(k-1, t\alpha_{min}) - \Gamma(k-1, t\alpha_{max})\}, \end{aligned} \tag{22}$$

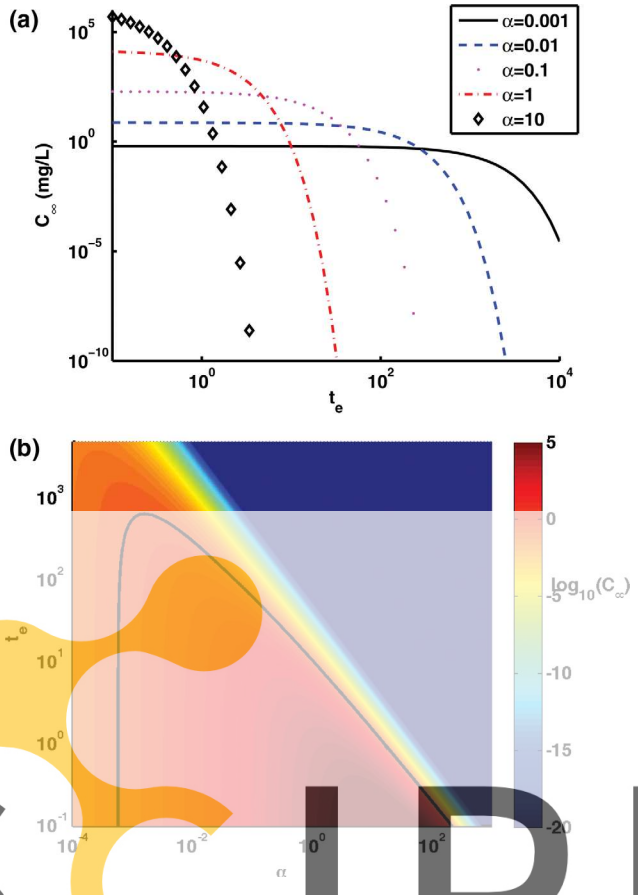

Figure 2. (top) Evolution of C_∞ (mg L^{-1}) with t_e (days) for several values of α_o (d^{-1}). (bottom) Contour plot of $\log_{10}(C_\infty)$ for various α_o and t_e. The parameter values used are listed in Table 1. The bold iso-contour line corresponds to $C_\infty = 0.35$ mg L^{-1}.

where $\theta_{\text{im}}^{\text{tot}}$ is the total immobile zone porosity, and $\Gamma(z, a)$ is the incomplete Gamma function. Differentiating $g(t)$ and substituting in equation (15) yield

$$C_\infty = \frac{m_o \theta_{\text{im}}^{\text{tot}} \mathcal{A}}{\theta_{\text{tot}}} [W_1 - t_{\text{adv}} (W_2 + W_3)], \tag{23}$$

where W_1, W_2, and W_3 are given by

$$\begin{aligned} W_1 &= t_e^{1-k} \{(\Gamma(k-1, t\alpha_{\min}) - \Gamma(k-1, t\alpha_{\max}))\} \\ W_2 &= (1-k) t_e^{-k} \{(\Gamma(k-1, t_e\alpha_{\min}) - \Gamma(k-1, t\alpha_{\max}))\} \\ W_3 &= t_e^{-1} \{a_{\max}^{k-1} e^{-t_e a_{\max}} - a_{\min}^{k-1} e^{-t_e a_{\min}}\}. \end{aligned} \tag{24}$$

[47] This result shares some common features with the single-rate solution. For example, the rebound concentration is proportional to m_o and $\theta_{\text{im}}^{\text{tot}}/\theta_{\text{tot}}$ for the same reasons as discussed above. It is also directly proportional to $\mathcal{A}$ (see equation (21)). This is analogous to C_∞ being directly proportional to α for the single-rate case; that is, when A is larger there is more weight in the larger exchange rates thus increasing the initial proportionality.

[48] The top half of Figure 3 illustrates how C_∞ varies with t_e for different power-law slopes (k). As for the single-rate case, there is a transition from smaller t_e (where larger k means larger C_∞) to larger t_e (where smaller k yields smaller C_∞).

[49] Juxtaposition of Figures 2 and 3 allows one to visualize the impact of the memory function on the interplay between C_∞ on t_e. For the power-law model, we have a more pronounced and distributed variation in C_∞ with respect to t_e. We observe that for smaller t_e, there appears to be a power-law decay at one rate, followed by a slower but still power-law decay rate at intermediate times and finally, a sudden exponential drop off at later times. For the single-rate model, C_∞ appears to maintain a more or less constant *plateau* at early times until it reaches a threshold value for t_e where it starts to decrease in a steep (exponential) manner.

[50] The contour plot in Figure 3 (bottom) depicts C_∞ for various t_e and k. Much like the single-rate case the nonmonotonicity with k is evident with a peak in values around $k = 2$. The black solid line corresponds to a constant value of C_∞ that visually depicts the nonmonotonic nature nicely. This behavior suggests that uncertainty in k may lead to a significant uncertainty in the assessment of risk for a particular problem.

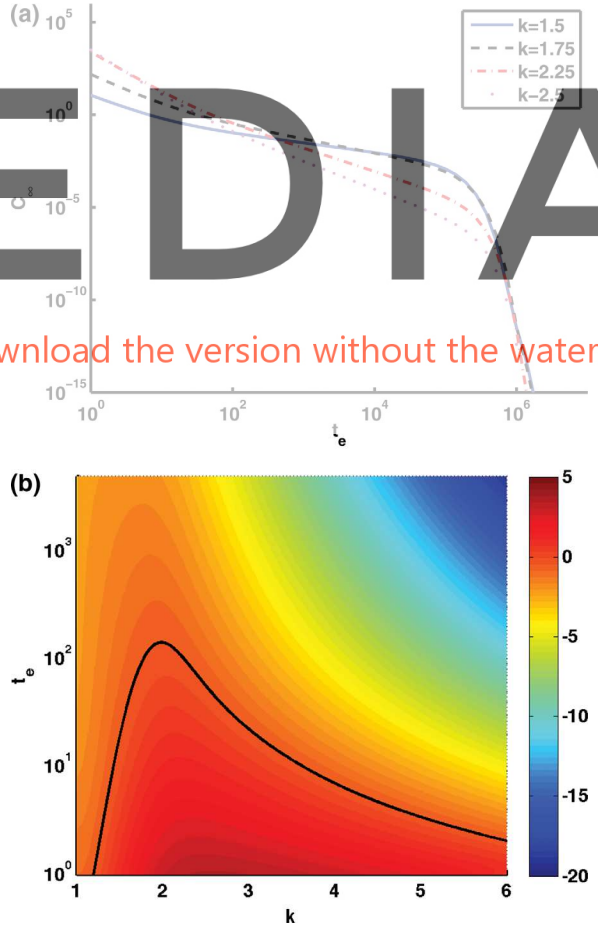

Figure 3. (top) Evolution of C_∞ (mg L^{-1}) with t_e (days) for several values of k. (bottom) Contour plot of $\log_{10}(C_\infty)$ for various k and t_e. The parameter values used are listed in Table 1 together with $\alpha_{\min} = 1 \times 10^{-5}$ d^{-1} and $\alpha_{\max} = 1 \times 10^3 d^{-1}$. The bold iso-contour line corresponds to $C_\infty = 0.35$ mg L^{-1}.

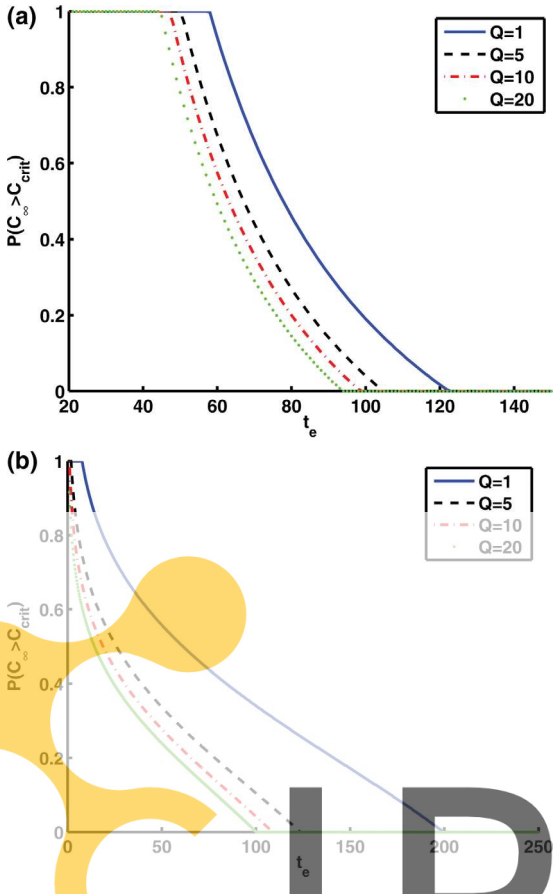

Figure 4. Probability of $C_\infty \geq C_{\text{crit}}$ (mg L^{-1}) versus t_e (days) for various values of $Q = 1$, 5, 10, and 20 m^3 d^{-1}. (top) Risk obtained for a single-rate model. For this plot, α_o was considered uncertain and uniformly distributed $\alpha_o \approx$ Uniform $[0.08, 0.2]$. (bottom) Risk obtained for a power-law model. For this plot, we assumed that $k \approx$ Uniform $[1.2, 1.8]$. Parameter values are listed in Table 1, and $C_{\text{crit}} = 5 \times 10^{-3}$ mg L^{-1}.

5. Risk Analysis and Uncertainty Quantification

[51] The parameters controlling the closed-form solutions provided in the previous sections are typically uncertain. For example, the total mass of the released pollutant, the area affected by the contamination, the initial conditions (young or old contamination), and the parameters controlling mass transfer properties are seldom known with absolute certainty.

[52] Measures of these uncertainties can be obtained from expert opinion through a variety of statistical inference techniques [*Rubin*, 2003, chap. 13] or estimated based on the observed decrease of concentration during pumping operations at the contaminated site. In this section, we show that the derived analytical solutions can actually be used to transfer these inherent parameter uncertainties into risk of remediation failure. Risk is defined as the probability of concentration exceeding a critical value (see equation (1)). Knowing that equations (15) and (18) express C_∞ as a function of model parameters, one can directly estimate the PDF of C_∞ by performing a variable transformation for random variables [see *Stone*, 1996, pp. 60–68]. The PDF of the rebound concentration C_∞ is denoted here by $p_c(C_\infty)$.

5.1. Dependence of the Risk on the Memory Function, Pumping Rates, and Operation Times

[53] Figure 4 illustrates the risk, defined as $\Pr[C_\infty \geq C_{\text{crit}}]$ (equation (1)), versus t_e for a young contaminated site for various values of Q. For the results in Figure 4, we set $C_{\text{crit}} = 5 \times 10^{-3}$ mg L^{-1}. Figure 4 (top) provides the evaluation of risk using a single-rate mass transfer model, while Figure 4 (bottom) corresponds to the power-law model. In the single-rate case, we assumed that α_o is uncertain and uniformly distributed $\alpha_o \approx$ Uniform $[0.08, 0.2]$. For the power-law model, k is considered uncertain with $k \approx$ Uniform $[1.2, 1.8]$.

[54] As shown in Figure 4, quantifying the uncertainty in C_∞ and the probability of exceeding a regulatory threshold value are important in order to decide how long to operate the pump such that C_∞ is kept below C_{crit} within an acceptable risk level. Fixing a pumping end-time (t_e) in both plots in Figure 4, we note that higher risks are associated with smaller pumping rates. Also, as expected, with increasing t_e for a given Q value, the risk given in equation (1) decreases. However, note that the rate at which the risk decreases strongly depends on the shape of the memory function as well as on the uncertainty of its parameters (i.e., k, α_o, etc.).

[55] A key element in evaluating the risk curves in Figure 4 lies in quantifying the PDF of C_∞, denoted by p_c. Therefore, analyzing the factors that control p_c will allow us to better grasp the mechanisms dictating the risk decay rate as a function of t_e. In the following, we provide a closed-form solution for the p_c for the specific case of a single-rate mass transfer model.

5.2. Rebound Concentration PDF

5.2.1. Uncertain Single-Rate Mass Transfer Coefficient

[56] Consider the case of a young contaminated site (see equation (20)). Suppose also that the single-rate mass transfer model is applicable at the site. Single-rate models are widely employed and provide a simple interpretation of the physics involved [e.g., *van Genuchten and Dalton*, 1986].

[57] We consider the single-rate mass transfer coefficient (α_o) to be uncertain with PDF p_α. Figure 5 shows the nonmonotonic relationship between C_∞ and α_o as given by equation (20) (see also Figure 2). This is due to the fact that for small α_o the mass is slowly released from the immobile region and therefore trapped in this region even after pumping. In this regime and for a given time of pumping, C_∞ will increase linearly with α_o. In contrast, for large values of α_o, the system is fully mixed and the mass can transfer rapidly from the immobile region when pumping, thereby leading to lower rebound conditions ($C_\infty \to 0$).

[58] Looking at Figure 5 it should be noted that $C_\infty(\alpha_o)$ can only be inverted by parts (in this case, two parts). This is due to the nonmonotonicity of $C_\infty(\alpha_o)$. Let us denote these two inverse functions as $\alpha_o = a_1(C_\infty)$ and

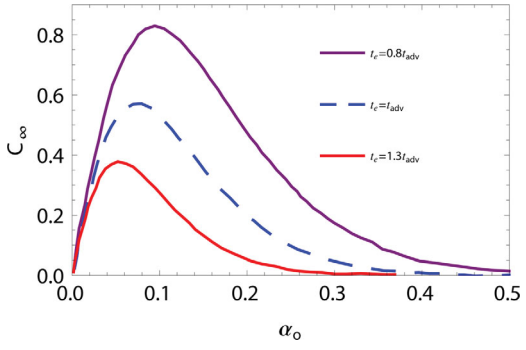

Figure 5. Rebound concentration C_∞ (mg L^{-1}) versus the single-rate mass transfer coefficient α_o (d^{-1}) for different pumping end-times t_e (days).

$\alpha_o = a_2(C_\infty)$. Then, to obtain p_c, we need the univariate change of variable transformation

$$p_c(C_\infty) = \left|\frac{\partial}{\partial \alpha_o}[C_\infty(a_1(C_\infty))]\right|^{-1} p_\alpha(a_1(C_\infty)) + \left|\frac{\partial}{\partial \alpha_o}[C_\infty(a_2(C_\infty))]\right|^{-1} p_\alpha(a_2(C_\infty)). \quad (25)$$

[59] One needs to first calculate the inverse functions a_1 and a_2 and then the derivative of C_∞ with respect to the uncertain parameters (in this case, α_o) to obtain p_c. This approach was, for example, used by *Sanchez-Vila et al.* [2009] to derive the PDF in reactive solute transport [see also *Tartakovsky et al.*, 2009]. The derivative can be analytically obtained as

$$\frac{\partial C_\infty}{\partial \alpha_o} = \frac{m_o \theta^o_{\text{im}}}{\theta_{\text{tot}}}[1 + 2\alpha_o t_{\text{adv}} - \alpha_o t_e(1 + \alpha_o t_{\text{adv}})]\exp[-\alpha_o t_e], \quad (26)$$

and the functions a_1 and a_2 can be estimated by finding the two-zero roots of the following equation:

$$\mathcal{F}(\alpha_o) = C_\infty - \frac{m_o \alpha_o \theta^o_{\text{im}}}{\theta_{\text{tot}}}(1 + \alpha_o t_{\text{adv}})\exp[-\alpha_o t_e]. \quad (27)$$

[60] The rebound concentration PDF can be evaluated by substituting equation (26) into equation (25) together with a prescribed assumed (or inferred) model for p_α.

5.2.2. Illustration

[61] Let α_o be uniformly distributed, $\alpha_o \approx$ Uniform$[\alpha_{o,\min}, \alpha_{o,\max}]$ where $\alpha_{o,\min}$ and $\alpha_{o,\max}$ represent lower and upper bounds on α_o, respectively. The values for $\alpha_{o,\min}$ and $\alpha_{o,\max}$ can be based on prior information or expert opinion. For our illustration, we opted for the uniform distribution; however, there are several methods available that allows one to estimate a prior PDF for α_o [*Kitanidis*, 1986; *Woodbury and Ulrych*, 2000; *Hou and Rubin*, 2005; *Kitanidis*, 2012]. Using p_α along with equations (25) and (26), we can estimate p_c.

[62] Figure 6 shows p_c for different pumping times (t_e). The parameter values used are those listed in Table 1. Results illustrate that p_c follows a U shape with two clear asymptotes that closely resembles a Beta-PDF with shape parameters less than unity. The latter result is consistent with the initial findings of *Bellin and Tonina* [2007] and frequently found later in a number of publications for different transport conceptual models and problem configurations. The asymptotes obtained in our case correspond to the two situations in which the derivative of C_∞ with respect to α_o is zero. These are the peak and the tail of the C_∞ distribution associated with large α_o values (Figure 5). In our case, the prior associated with α_o expands over a large range so that the asymptotes are clearly depicted. It is worth mentioning that for other situations, smaller priors can truncate the left asymptote (controlled by $\alpha_{o,\max}$) and result in discontinuities in the PDF (when a_1 is different than a_2). If the duration of pumping increases, the range of possible values that C_∞ can attain decrease.

[63] In a similar fashion, for a given end-time of pumping t_e, one can analytically estimate the risk of exceeding a critical concentration. With the aid of equation (25), equation (1) can be rewritten as

$$\text{Risk} = \Pr[C_\infty \geq C_{\text{crit}}] = 1 - \int_0^{a_1(C_{\text{crit}})} p_\alpha(\alpha_o)\mathrm{d}\alpha_o - \int_{a_2(C_{\text{crit}})}^{\infty} p_\alpha(\alpha_o)\mathrm{d}\alpha_o. \quad (28)$$

or simply,

$$\text{Risk} = 1 - I_1(C_{\text{crit}}) - I_2(C_{\text{crit}}), \quad (29)$$

where we have the following explicit solutions for I_1 and I_2 (given a uniform PDF model for p_α):

$$I_1(C_{\text{crit}}) = \begin{cases} \dfrac{a_1(C_{\text{crit}}) - \alpha_{o,\min}}{\alpha_{o,\max} - \alpha_{o,\min}}, & a_1(C_{\text{crit}}) > \alpha_{o,\min} \\ 0 & \text{otherwise} \end{cases} \quad (30)$$

$$I_2(C_{\text{crit}}) = \begin{cases} \dfrac{\alpha_{o,\max} - a_2(C_{\text{crit}})}{\alpha_{o,\max} - \alpha_{o,\min}}, & a_2(C_{\text{crit}}) < \alpha_{o,\max} \\ 0 & \text{otherwise} \end{cases}. \quad (31)$$

[64] The dependence of risk on C_{crit} and end-time of pumping is illustrated in Figure 7. Our results show that the risk tends to decrease with t_e following a power-law behavior with slope close to −1. Afterward, a sudden drop in risk occurs. The pumping time needed for this situation to occur

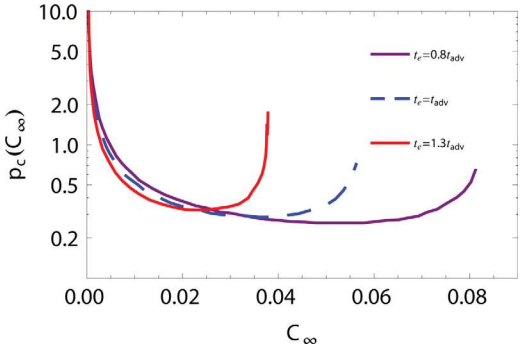

Figure 6. PDF for the rebound concentration $p_c(C_\infty)$ evaluated at different values of $t_e = 0.8t_{\text{adv}}$, t_{adv}, and $1.3t_{\text{adv}}$ days.

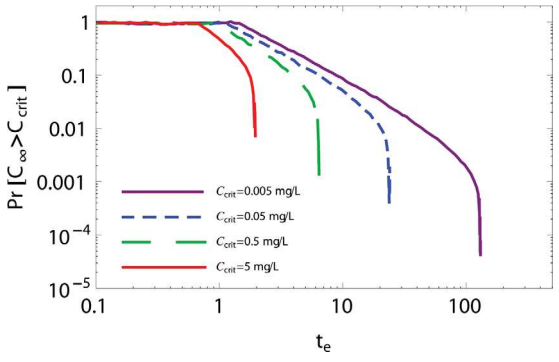

Figure 7. Risk versus the end-time of pumping t_e (days) for different C_{crit} (mg L^{-1}). Risk is defined as $\Pr[C_\infty \geq C_{\text{crit}}]$ (see equation (1)).

(i.e., the sudden drop in the evaluated risk) is actually the time needed for C_∞ to approach C_{crit}. When this happens, a_1 approaches a_2 and $I_1 + I_2 = 1$ such that the risk approaches zero (see equation (29)).

[65] For a given contaminant and corresponding critical concentration C_{crit}, we can estimate the time needed to obtain this sudden drop of risk by estimating the time t_e needed for $C_\infty(\alpha_p)$ to approach C_{crit}, i.e.,

$$C_{\text{crit}} = \frac{m_o \theta^o_{\text{im}}}{\theta_{\text{tot}}} \alpha_p (1 + \alpha_p t_{\text{adv}}) \exp[-\alpha_p t_e], \tag{32}$$

where α_p is given by

$$\alpha_p = \frac{\zeta + \sqrt{\zeta^2 + 4\vartheta}}{2\vartheta} \text{ with}$$
$$\zeta = t_{\text{adv}} + \frac{m_o \theta^o_{\text{im}}}{\theta_{\text{tot}}}(t_{\text{adv}} - t_e); \tag{33}$$
$$\vartheta = \frac{m_o \theta^o_{\text{im}}}{\theta_{\text{tot}}} t_{\text{adv}} t_e.$$

[66] This relationship between C_{crit} and the necessary t_e to reduce the risk to its minimum expression is shown in Figure 8. Here t_e is normalized by t_{adv}. In Figure 8, we can clearly distinguish two separate regimes. For $t_e < t_{\text{adv}}$, C_{crit} rapidly decreases following a power-law behavior with a slope of -2. Once $t_e > t_{\text{adv}}$ the slope changes to a value of -1, and the time needed to reduce the risk increases. This is consistent with our conceptual model of mass transfer. If mass transfer is important and critical concentrations are relatively large, then it is possible to cleanup the aquifer by direct pumping. However, for very toxic contaminants with small C_{crit} values, the mass remaining in the immobile regions becomes critical, ultimately increasing the time needed for pumping.

[67] Up to now, results were obtained for a young contaminated site. Now we compare an old contaminated site versus a young contaminated site. In the case of an old contaminated site, the approach used to obtain p_c and $\Pr[C_\infty > C_{\text{crit}}]$ is analogous with the exception that we employ equation (18) as a starting point.

[68] To determine the initial concentration C_o in both immobile and mobile regions for the old contaminated site scenario based on the data given in Table 1, we use $M = C_o \pi R^2 b \phi = Q m_o$ (where M denotes mass). For the parameters used, this gives $C_o = 0.018$ kg m^{-3}.

[69] Figure 9 compares p_c for old contaminated sites against young contaminated sites at $t_e = t_{\text{adv}}$. Notably, old contaminations are shown to be difficult to cleanup, having large C_∞ occurs with greatest probability. The C_∞-PDF still shows the U shape with two asymptotes. The left asymptote remains almost the same as for young contaminated sites. It corresponds to large mass transfer coefficients (fully mixed system) in which the immobile region does not effectively exist.

[70] Figure 10 shows how the risk varies with t_e for an old and young site contaminated by a toxic compound of $C_{\text{crit}} = 0.05$ mg L^{-1}. As expected, an old contaminated site poses a more severe contamination problem with a higher risk of C_∞ exceeding C_{crit}. As expected, results show that an old contaminated site will require longer pumping times to reach the same level of risk.

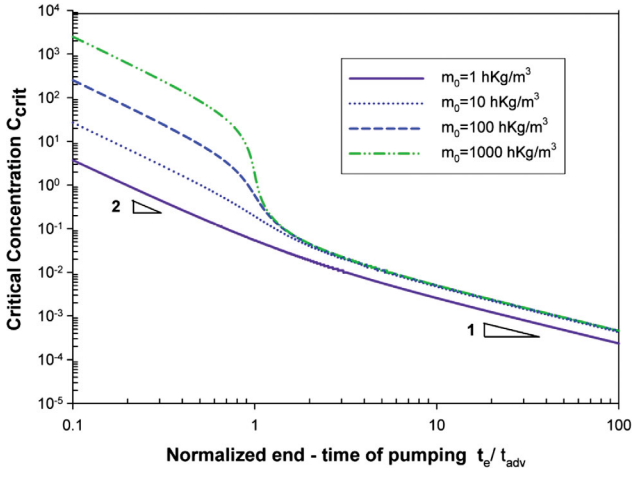

Figure 8. Illustrating the dependency between the critical concentration and the normalized end-time of pumping (t_e/ t_{adv}) for different values of the zeroth-order moment of the breakthrough curve m_o (h kg m^{-3}). Results show the changes of the slope when t_e approaches t_{adv}.

5.2.3. Accounting for Uncertainty in Other Parameters

[71] Results obtained so far only consider one source of uncertainty in α_o. In practice, other important parameters such as the initial mass and/or the volume affected by the

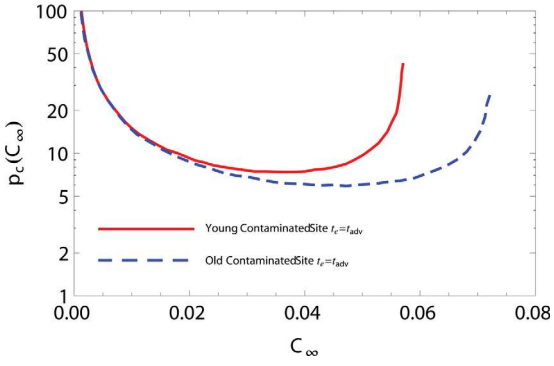

Figure 9. PDF for the rebound concentration $p_c(C_\infty)$ for an old and young contaminated site (see equations (15) and (18)).

pollution may also be uncertain. In those cases, the methodology remains the same with a slight modification in the rule of random variable transformation. Let us consider that the field capacity $\beta = \theta_{\text{im}}/\theta_{\text{tot}}$ is also uncertain. To illustrate this, let us also assume that α_o and β are two independent random variables. Furthermore, for the sake of simplicity, we consider β be uniformly distributed between $\beta_{\min}$ and $\beta_{\max}$ with PDF $p_\beta(\beta)$. Under these conditions, we can formulate the following PDF for C_∞:

$$p_c(C_\infty) = \frac{1}{\beta_{\max} - \beta_{\min}} \int_{\beta_{\min}}^{\beta_{\max}} \left| \frac{\partial}{\partial \alpha_o} [C_\infty(a_1(C_\infty;\beta))] \right|^{-1} \times p_\alpha(a_1(C_\infty))\mathrm{d}\beta + \frac{1}{\beta_{\max} - \beta_{\min}} \int_{\beta_{\min}}^{\beta_{\max}} \times \left| \frac{\partial}{\partial \alpha_o} [C_\infty(a_2(C_\infty;\beta))] \right|^{-1} p_\alpha(a_2(C_\infty))\mathrm{d}\beta. \quad (34)$$

[72] It is important to note that other types of distributions for the uncertain parameters can be used. Depending on the complexity of the uncertain parameter PDF, numerical integration may be required. Therefore, the procedure described in this paper is not limited to our choice of prior. As will be shown in the next section, the choice of the prior PDF is crucial. The method above can also take into account multiple-correlated random variables.

6. Application and Field Data

[73] In this section, we aim to show the potential of the risk-based probabilistic framework and how it could be used in applications. Here we test the performance of the simple risk-based concentration rebound model described in the previous sections against field data. The data used for comparison are taken from a controlled pulsed pump-and-treat remediation field experiment performed at the Dover Air Force Base, USA [*MacKay et al*., 2000]. The aquifer consists of a medium-to-coarse sand, sometimes intermixed with clay lenses. The bottom of the aquifer overlies an aquitard that separates the Columbia and Frederica aquifers. The experimental site contains several dissolved plumes that occurred due to the depletion of an upgradient dense nonaqueous phase liquid (DNAPL) source contamination believed to have occurred 25–50 years before the experiment.

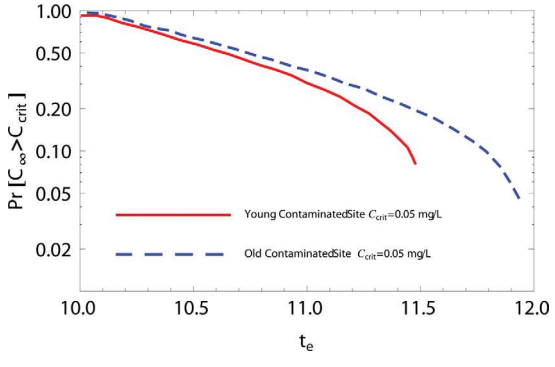

Figure 10. Risk versus the end-time of pumping t_e (days) for an old (equation (18)) and young (equation (15)) contaminated site for $C_{\text{crit}} = 0.05$ mg L^{-1}. Risk is defined as $\Pr[C_\infty \geq C_{\text{crit}}]$ (see equation (1)).

[74] The experiment was designed to investigate the efficiency and advantages of a pulsed-pumping strategy compared to continuous extraction during the application of a pump-and-treat remediation scheme. Here, we will focus only on the pulsed-pumping strategy results to be able to compare our risk analysis method with the rebound concentrations obtained after the pumping cycle. Sheet pile test cells were used to isolate the plumes in a controlled environment. A battery of injection and extraction wells was then placed inside the cell to flush the system with pumping cycles. The experiment provides a realistic field setting that is well suited for our purposes and will allow us to illustrate the applicability of our probabilistic framework. In this field experiment, diffusive concentration rebounding from a less permeable region (mainly the aquitard) was observed to control the elution curves for PCE, TCE, and c-DCE. Moreover, the selected experimental site was located far away from the source zone so that free DNAPL phase was not present; monitored biotransformation processes were observed to be negligible for the 9 month duration of the field experiment. We note that the flow configuration is fundamentally different from the main scenario previously presented in this paper. This helps us highlight a strength of the methodology which essentially depends on travel times but not on the specific underlying flow configuration.

[75] Figure 19b of *MacKay et al*. [2000] provides the breakthrough curve for c-DCE from the Dover Site (prior to and during the pumping phase and after pumping ceases). For completeness, Figure 11 replicates the data from Figure 19b of *MacKay et al*. [2000]. Based on the information given in *MacKay et al*. [2000], we were able to obtain rough estimates for the following parameters that will serve as inputs for the model. Consistent with the double porosity approach, the upscaled model considers the coexistence of a permeable region (the aquifer) and a less permeable region (the aquitard). The aquifer is approximately 11 m in depth, while the aquitard thickness is about 2 m. Knowing that the porosity in the aquifer and the aquitard are about 0.34 and 0.545, respectively, this yields $\theta_m \approx 0.28$, $\theta_{\text{im}} \approx 0.08$, and $\theta_{\text{tot}} \approx 0.37$. Other relevant parameters estimated from *MacKay et al*. [2000] are $b \approx 13$ m, $t_e = 27$ days, and $Q \approx 3.55$ m^3 d^{-1}. An estimated value $m_o \approx 49{,}600$ d µg m^{-3} was obtained from the c-DCE breakthrough curve (assuming the system was in equilibrium). All the values mentioned above were taken from *MacKay et al*. [2000] or else inferred from the information found in the text and Figures 17b and 19b of *MacKay et al*. [2000]. Based on the same breakthrough curves, the travel time is approximately 10 days, and $C_o \approx 5531$ µg L^{-1}. The only information that was not directly available in this paper was the mass transfer coefficient parameters of the memory function. It is very important to note that this analysis is only meant to provide a rough comparison given the absence of more precise information. It primarily serves to illustrate the probabilistic risk framework put forth in this work that can be used when uncertainty prevails. It is under these conditions that probabilistic tools are needed and uncertainty quantification cannot be ignored [see *Rubin*, 2003, chaps. 1–2].

[76] Given the lack of additional site information, we opt to perform the comparison using the single-rate model.

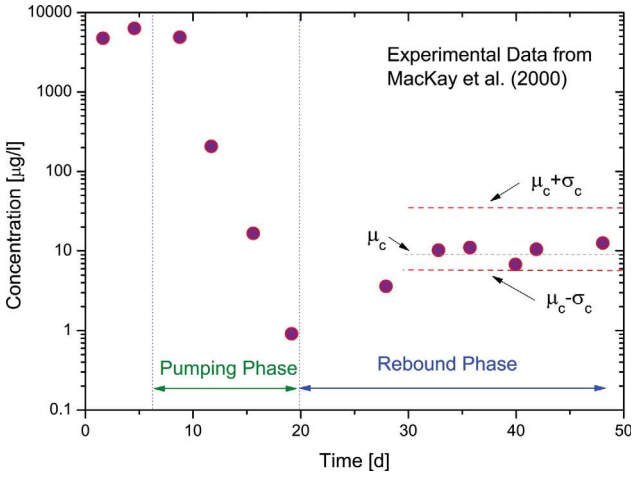

Figure 11. Data taken from Figure 19b of *MacKay et al*. [2000]. The temporal mean μ_c and standard deviation σ_c of the rebound concentration data (rebound phase) are marked.

Using the breakthrough data obtained during the pumping regime in Figures 17b and 19b of *MacKay et al*. [2000], we performed a simple linear fit to estimate the single-rate mass transfer coefficient. The result of the fitting process varied since it depends on the number of data points and the portion of the breakthrough used for the estimation [see *MacKay et al*., 2000, Figures 17b and 19b]. The smallest estimated mass transfer coefficient value was $\alpha_o \approx 0.055$ d^{-1}, and the largest was $\alpha_o \approx 1.15 d^{-1}$. Because of the uncertainty in α_o, we assume that it is uniformly distributed, $\alpha_o \approx$ Uniform[0.055,1.15].

[77] Since the Dover Site has been contaminated for many years, we choose to classify it as an old contaminated site. Therefore, using the single-rate mass transfer model in equation (18), we obtain the following solution:

$$C_\infty = \frac{m_o}{\theta_{\text{tot}}}\left\{\alpha_o\theta^o_{\text{im}}\exp[-\alpha_o t] + t_{\text{adv}}\,\alpha_o^2\theta^o_{\text{im}}\exp[-\alpha_o t]\right\} + C_o\theta^o_{\text{im}}\exp[-\alpha_o t] + t_{\text{adv}}\,\alpha_o C_o\theta^o_{\text{im}}\exp[-\alpha_o t]. \quad (35)$$

[78] We test our probabilistic predictions of C_∞ against the temporal statistics of the concentration data from the resting phase depicted in Figure 11. Specifically, we depict the mean $\left(\mu_c \approx 9.14\ \mu\text{g L}^{-1}\right)$ and standard deviation $\left(\sigma_c \approx 3.03\ \mu\text{g L}^{-1}\right)$ of the rebound phase data (see Figure 11).

[79] Figure 12 depicts the estimated C_∞-PDF. From the C_∞-PDF, we quantified that the probability that C_∞ lies within the $\mu_c \pm 2\sigma_c$ confidence interval is equal to 8%. The mean value for C_∞ predicted from the PDF is approximately equal to 31 µg L^{-1} and therefore, larger than μ_c. This is consistent with the conservative formulation provided in equation (14). It is worth noting in Figure 12 that the most probable concentrations occur at the smallest concentrations. As shown in Figure 12, the μ_c and confidence interval are already in the low probability regime of the PDF. This PDF also allows us to quantify the probability of exceeding a critical concentration value, for example, the Prob$[C_\infty \geq 7\ \mu\text{g L}^{-1}] = 22\%$, which again demonstrates that almost 80% of the probable concentrations lie below this value.

[80] It is very important to note that the results shown here are entirely conditional on the parameter values estimated and in particular our choice of the prior PDF for α_o (uniform PDF). Uniform distributions are known to be the least informative type of prior but often used for practical reasons. The inference of priors is clearly beyond the scope of this paper, and we refer to *Rubin* [2003, chap. 13, and references therein] for more elaborate prior inference methodologies [see also *Kitanidis*, 1986; *Hou and Rubin*, 2005; *Kitanidis*, 2012]. Better estimates and updates of the α_o prior PDF would improve the performance of the model. Additionally, our assumption of a single-rate mass transfer model for this comparison could be relaxed as there is evidence in Figures 17b and 19b of *MacKay et al*. [2000] that the memory function would be best characterized by multiple rate mass transfer coefficients.

[81] Summarizing, our purpose in this section is to illustrate the potential of the probabilistic framework to estimate rebound concentration and corresponding uncertainties from a risk perspective. Evidently, as more information becomes available from the site, estimates of the model's input parameters and their corresponding uncertainty will be improved and lead to better predictions. The performance of the results is attributed to several factors: (i) we opted for the simplest prior distribution for α_o, (ii) neglected the uncertainty of other input parameters, and (iii) the choice of the memory function.

7. Summary and Final Remarks

[82] Assessment of the efficiency of any remediation technology prior to its application in the field is inherently cumbersome. Among the many difficulties, assessing the likelihood of occurrence of concentration rebound caused by back diffusion is a key factor. This fact has led the scientific community to think that the effectiveness of remediation technologies should be evaluated by the risk reduction that is achieved by their application [*Soga et al*.,

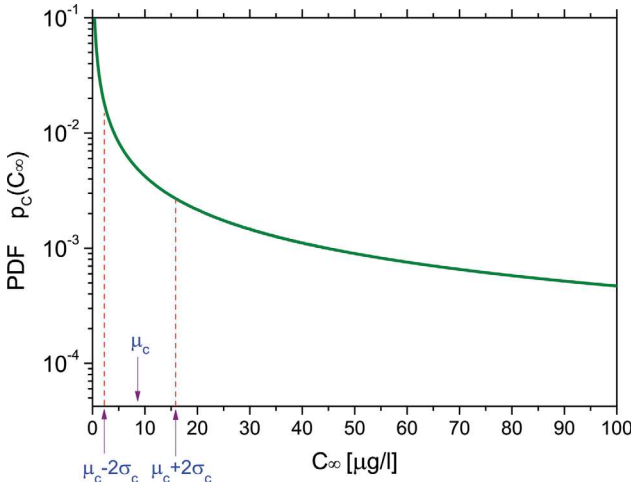

Figure 12. Rebound concentration PDF. Here μ_c and σ_c correspond to the mean and standard deviation of the rebound concentration data over the rebound phase marked in Figure 11. Rebound concentration data were taken from Figure 19b of *MacKay et al*. [2000].

2004]. Our goal was to employ a probabilistic framework that could be used to design optimal pumping tasks while accounting for the risk of rebound occurrence. Therefore, this paper dealt with the widely observed effect of the increase of registered concentration at the well after pumping ceases in a pump-and-treat remediation effort. The buildup of the concentration is attributed to the resident concentration around the well being much larger than the flux-averaged concentration at the well. While different processes may account for this phenomenon, we focus on natural heterogeneity. The role of spatial variability of the distribution of permeability on transport is modeled by means of an effective governing equation, i.e., the MRMT model.

[83] Based on a number of simplifying hypotheses, we generated a deterministic solution to obtain the concentration that would be observed at the well after a certain time t_e of pumping at a constant rate Q. The medium is characterized by a memory function and some information regarding the extent of pollution and the history of the contaminated site is required. As shown, the closed-form expressions are flexible and can be implemented within water resources management framework [*Bolster et al*., 2009; *de Barros et al*., 2011a; *Fernàndez-Garcia et al*., 2012]. Furthermore, the solutions presented in this work could be expanded to account for different types of memory function and multiple sources of uncertainty.

[84] Within their range of validity, our expressions can be employed to provide relatively simple a priori risk estimates. This has social, environmental, and economic implications when applied to real sites. The analytical expressions derived in this work may serve as a preliminary screening tool in order to allocate resources toward uncertainty reduction and model refinement (see detailed discussion in *de Barros and Rubin* [2008] and *de Barros et al*. [2011b]). The solutions provided need some information about the site and the geological formation. Such information can be obtained in terms of priors and with additional sampling can be updated using available statistical inference tools [e.g., *Hou and Rubin*, 2005]. In addition, the analytical expressions derived in this work provide the ability to obtain insights into many of the important factors that control the evolution of the risk curves. For instance, our results illustrate the importance that advective time plays in the risk decay curves as a function of both the target concentration (e.g., regulatory based) and the pumping operational time. We also showed how the risk-based framework could be used in applications by comparing our conservative stochastic predictions with field data taken from the Dover Site.

[85] Finally, we emphasize that the focus of our paper is not on the MRMT method used to estimate rebound concentrations but on the importance of considering within a single framework the *joint* effect of (i) the pumping operation and (ii) uncertainty quantification in estimating the risk of concentration rebounds. There are several existing methods [see *Neuman and Tartakovsky*, 2009, and references therein] that could be used within the proposed framework. The drawback of these upscaled models is that most of them rely on fitting parameters. There is an ongoing research effort that attempts to link these parameters with the actual heterogeneity of the aquifer [e.g., *Willmann et al*., 2008]. Regardless of the choice of method, this paper describes a novel risk-based framework for both longtime rebound concentrations and their corresponding uncertainty characterization.

[86] **Acknowledgments.** The support by the Spanish Ministry of Science through the Juan de la Cierva program is acknowledged. This work has been supported by the Spanish Ministry of Science and Innovation through the project Consolider-Ingenio 2010 CSD2009-00065 and FEAR CGL2012-38120. D.B. would like to express thanks for financial support via NSF grant EAR-1113704.

References

Bellin, A., and D. Tonina (2007), Probability density function of non-reactive solute concentration in heterogeneous porous formations, *J. Contam. Hydrol.*, *94*(1–2), 109–125.

Benson, D., R. Schumer, S. Wheatcraft, and M. Meerschaert (2001), Fractional dispersion, levy motion, and the made tracer tests, *Transp. Porous Media*, *42*, 211–240.

Berkowitz, B., A. Cortis, M. Dentz, and H. Scher (2006), Modeling non-Fickian transport in geological formations as a continuous time random walk, *Rev. Geophys.*, *44*, RG2003, doi:10.1029/2005RG000178.

Bolster, D., M. Barahona, M. Dentz, D. Fernandez-Garcia, X. Sanchez-Vila, P. Trinchero, C. Valhondo, and D. Tartakovsky (2009), Probabilistic risk analysis of groundwater remediation strategies, *Water Resour. Res.*, *45*, W06413, doi:10.1029/2008WR007551.

Carrera, J., X. Sánchez-Vila, I. Benet, A. Medina, G. Galarza, and J. Guimerà (1998), On matrix diffusion: Formulations, solution methods and qualitative effects, *Hydrogeol. J.*, *6*(1), 178–190.

Chen, W., and R. Wagenet (1995), Solute transport in porous media with sorption-site heterogeneity, *Environ. Sci. Technol.*, *29*(11), 2725–2734.

Cohen, R., A. Vincent, J. Mercer, C. Faust, and C. Spalding (1994), Methods for monitoring pump-and-treat performance, EPA/600/R-94/123, R.S. Kerr Environ. Res. Lab., Ada, Okla., 102 pp.

Cushman, J., and T. Ginn (1993), Nonlocal dispersion in media with continuously evolving scales of heterogeneity, *Transp. Porous Media*, *13*, 123–138.

de Barros, F., and Y. Rubin (2008), A risk-driven approach for subsurface site characterization, *Water Resour. Res.*, *44*, W01414, doi:10.1029/2007WR006081.

de Barros, F., D. Bolster, X. Sanchez-Vila, and W. Nowak (2011a), A divide and conquer approach to cope with uncertainty, human health risk, and decision making in contaminant hydrology, *Water Resour. Res.*, *47*, W05508, doi:10.1029/2010WR009954.

de Barros, F., A. Fiori, and A. Bellin (2011b), A simple closed-form solution for assessing concentration uncertainty, *Water Resour. Res.*, *47*, W12603, doi:10.1029/2011WR011107.

Dentz, M., and B. Berkowitz (2003), Transport behavior of a passive solute in continuous time random walks and multirate mass transfer, *Water Resour. Res.*, *39*(5), 1111, doi:10.1029/2001WR001163.

Donado, L., X. Sánchez-Vila, M. Dentz, J. Carrera, and D. Bolster (2009), Multicomponent reactive transport in multicontinuum media, *Water Resour. Res.*, *45*, W11402, doi:10.1029/2008WR006823.

Fernàndez-Garcia, D., G. Llerar-Meza, and J. Gómez-Hernández (2009), Upscaling transport with mass transfer models: Mean behavior and propagation of uncertainty, *Water Resour. Res.*, *45*, W10411, doi:10.1029/2009WR007764.

Fernàndez-Garcia, D., D. Bolster, X. Sanchez-Vila, and D. Tartakovsky (2012), A Bayesian approach to integrate temporal data into probabilistic risk analysis of monitored NAPL remediation, *Adv. Water Resour.*, *36*, 108–120.

Gouze, P., Y. Melean, T. Le Borgne, M. Dentz, and J. Carrera (2008), Non-Fickian dispersion in porous media explained by heterogeneous microscale matrix diffusion, *Water Resour. Res.*, *44*, W11416, doi:10.1029/2007WR006690.

Haggerty, R., and S. Gorelick (1995), Multiple-rate mass transfer for modeling diffusion and surface reactions in media with pore-scale heterogeneity, *Water Resour. Res.*, *31*(10), 2383–2400.

Haggerty, R., S. W. Fleming, and S. A. McKenna (2000a), ''STAMMT-R: Solute transport and multirate mass transfer in radial coordinates, Version 1.01, Rep.''. *SAND99*, *164* (2000).

Haggerty, R., S. McKenna, and L. Meigs (2000b), On the late-time behavior of tracer test breakthrough curves, *Water Resour. Res.*, *36*(12), 3467–3479.

Haggerty, R., S. Fleming, L. Meigs, and S. McKenna (2001), Tracer tests in a fractured dolomite: 2. analysis of mass transfer in single-well injection-withdrawal tests, *Water Resour. Res.*, *37*(5), 1129–1142.

Harvey, C., R. Haggerty, and S. Gorelick (1994), Aquifer remediation: A method for estimating mass transfer rate coefficients and an evaluation of pulsed pumping, *Water Resour. Res.*, *30*(7), 1979–1991.

Hou, Z., and Y. Rubin (2005), On minimum relative entropy concepts and prior compatibility issues in vadose zone inverse and forward modeling, *Water Resour. Res.*, *41*, W12425, doi:10.1029/2005WR004082.

Kitanidis, P. (1986), Parameter uncertainty in estimation of spatial functions: Bayesian analysis, *Water Resour. Res.*, *22*(4), 499–507.

Kitanidis, P. (2012), Generalized priors in Bayesian inversion problems, *Adv. Water Resour.*, *36*, 3–10.

Kreft, A., and A. Zuber (1978), On the physical meaning of the dispersion equation and its solutions for different initial and boundary conditions, *Chem. Eng. Sci.*, *33*(11), 1471–1480.

Lawrence, A., X. Sanchez-Vila, and Y. Rubin (2002), Conditional moments of the breakthrough curves of kinetically sorbing solute in heterogeneous porous media using multirate mass transfer models for sorption and desorption, *Water Resour. Res.*, *38*(11), 1248, doi:10.1029/2001WR001006.

Luo, J., O. Cirpka, W. Wu, M. Fienen, P. Jardine, T. Mehlhorn, D. Watson, C. Criddle, and P. Kitanidis (2005), Mass-transfer limitations for nitrate removal in a uranium-contaminated aquifer, *Environ. Sci. Technol.*, *39*(21), 8453–8459.

Luo, J., W. Wu, M. Fienen, P. Jardine, T. Mehlhorn, D. Watson, O. Cirpka, C. Criddle, and P. Kitanidis (2006), A nested-cell approach for in situ remediation, *Ground Water*, *44*(2), 266–274.

Ma, R., C. Zheng, H. Prommer, J. Greskowiak, C. Liu, J. Zachara, and M. Rockhold (2010), A field-scale reactive transport model for U(VI) migration influenced by coupled multirate mass transfer and surface complexation reactions, *Water Resour. Res.*, *46*, W05509, doi:10.1029/2009WR008168.

Mackay, D., and J. Cherry (1989), Groundwater contamination: Pump-and-treat remediation, *Environ. Sci. Technol.*, *23*(6), 630–636.

MacKay, D., R. Wilson, M. Brown, W. Ball, G. Xia, and D. Durfee (2000), A controlled field evaluation of continuous vs. pulsed pump-and-treat remediation of a voc-contaminated aquifer: Site characterization, experimental setup, and overview of results, *J. Contam. Hydrol.*, *41*(1–2), 81–131.

Margolin, G., M. Dentz, and B. Berkowitz (2003), Continuous time random walk and multirate mass transfer modeling of sorption, *Chem. Phys.*, *295*, 71–80.

Maxwell, R., S. Carle, and A. Tompson (2008), Contamination, risk, and heterogeneity: On the effectiveness of aquifer remediation, *Environ. Geol.*, *54*(8), 1771–1786.

McKenna, S., L. Meigs, and R. Haggerty (2001), Tracer tests in a fractured dolomite: 3. Double-porosity, multiple-rate mass transfer processes in convergent flow tracer tests, *Water Resour. Res.*, *37*(5), 1143–1154.

Meigs, L., and R. Beauheim (2001), Tracer tests in a fractured dolomite: 1. Experimental design and observed tracer recoveries, *Water Resour. Res.*, *37*(5), 1113–1128.

Morales-Casique, E., S. Neuman, and A. Guadagnini (2006), Nonlocal and localized analyses of nonreactive solute transport in bounded randomly heterogeneous porous media: Theoretical framework, *Adv. Water Resour.*, *29*, 1238–1255.

Neuman, S., and D. Tartakovsky (2009), Perspective on theories of non-Fickian transport in heterogeneous media, *Adv. Water Resour.*, *32*, 670–680.

National Research Council (1994), *Alternatives for Ground Water Cleanup*, Natl. Acad., Washington, D. C.

Rubin, Y. (2003), *Applied Stochastic Hydrogeology*, Oxford Univ. Press, Oxford.

Sanchez-Vila, X., A. Guadagnini, and D. Fernàndez-Garcia (2009), Conditional probability density functions of concentrations for mixing-controlled reactive transport in heterogeneous aquifers, *Math. Geosci.*, *41*(3), 323–351.

Silva, O., J. Carrera, M. Dentz, S. Kumar, A. Alcolea, and M. Willmann (2009), A general real-time formulation for multi-rate mass transfer problems, *Hydrol. Earth Syst. Sci.*, *13*(8), 1399–1411.

Soga, K., J. Page, and T. Illangasekare (2004), A review of NAPL source zone remediation efficiency and the mass flux approach, *J. Hazard. Mater.*, *110*(1–3), 13–27.

Stone, C. (1996), *A course in probability and statistics*, Duxbury Press, Belmont.

Tartakovsky, D., M. Dentz, and P. Lichtner (2009), Probability density functions for advective-reactive transport with uncertain reaction rates, *Water Resour. Res.*, *45*, W07414, doi:10.1029/2008WR007383.

U.S. Environmental Protection Agency (2001), Risk assessment guidance for Superfund, vol. III, Part A: Process for conducting probabilistic risk assessment, Tech. Rep. EPA 540/R-02/002, Washington, D. C.

van Genuchten, M., and F. Dalton (1986), Models for simulating salt movement in aggregated field soils, *Geoderma*, *38*(1–4), 165–183.

van Genuchten, R., and J. Parker (1984), Flux-averaged and volume averaged concentrations in continuum approaches to solute transport, *Water Resour. Res.*, *20*(7), 866–872.

Willmann, M., J. Carrera, and X. Sánchez-Vila (2008), Transport upscaling in heterogeneous aquifers: What physical parameters control memory functions?, *Water Resour. Res.*, *44*, W12437, doi:10.1029/2007WR006531.

Willmann, M., J. Carrera, X. Sánchez-Vila, O. Silva, and M. Dentz (2010), Coupling of mass transfer and reactive transport for non-linear reactions in heterogeneous media, *Water Resour. Res.*, *46*, W07512, doi:10.1029/2009WR007739.

Woodbury, A., and T. Ulrych (2000), A full-Bayesian approach to the groundwater inverse problem for steady state flow, *Water Resour. Res.*, *36*(8), 2081–2093.

Zhang, Z., and M. Brusseau (1999), Nonideal transport of reactive solutes in heterogeneous porous media: 5. simulating regional-scale behavior of a trichloroethene plume during pump-and-treat remediation, *Water Resour. Res.*, *35*(10), 2921–2935.